scientific reports

Check for updates

OPEN

Efficient sorption and secure immobilization of strontium ions onto nanoporous alumino-borosilicate as a new matrix

Ali Abbasi[1], Armen Avanes[1], Reza Davarkhah[2], Ali Yadollahi[2] & Hamid Sepehrian[2]✉

The objective behind developing the nanoporous alumino-borosilicate (AlBS) was to remove strontium ion (Sr^{2+}) from liquid waste and subsequently stabilize it. The sorption capacity of the nanoporous AlBS was assessed in relation to various experimental factors, including contact time, temperature, initial pH solution, and initial concentration of Sr ions. According to the obtained results, nanoporous AlBS shows a maximum Sr^{2+} sorption capacity of 163.08 mg/g. In order to achieve stable immobilization of the sorbed Sr ions, heat treatments at different temperatures were applied to the Sr-containing nanoporous AlBS. Various eluents were used in the leach tests to examine the Sr ions leaching from heat-treated materials. Only 3.43% of the Sr ions initially adsorbed in the nanoporous AlBS matrix was washed out with 1 M sodium chloride eluent, showing that heating the sample to around 1100 °C successfully trapped Sr ions in the nanoporous AlBS matrix.

Keywords Strontium, Sorption, Nanoporous, Alumino-borosilicate, Immobilization, Leaching

Proper management of liquid radioactive wastes is essential to minimize the potential for radionuclide release following disposal. Managing liquid waste in nuclear facilities focuses on two main goals: first, reducing volume for easier storage, and second, removing the radionuclides and their stable immobilization to avoid release into the surrounding environment[1]. Since the Fukushima nuclear accident, the Strontium (Sr) radionuclide has been considered as one of the most worrying radioactive hazards[2–4]. Strontium-90 has a half-life of 29 years and poses long-term environmental and health risks due to its radioactivity and high mobility[5]. The management of radioactive Strontium contamination, therefore, remains a critical issue in environmental safety and public health.

Non-radioactive Strontium is not highly toxic, but overexposure can cause bone growth issues in children. The main toxic effect of excessive Strontium in laboratory animals is abnormal skeletal development[6]. The primary source of stable Sr ions input into rivers or groundwater is the erosion of limestone or rocks containing celestite[7]. Sr ions was commonly found in natural water with low trace levels (less than 0.2 mg/L), although certain areas showed moderate (1–10 mg/L) to elevated Sr ions levels (over 10 mg/L) in natural water[8].

A review of literature on treating radioactive liquid wastes shows that different methods such as co-precipitation, evaporation, solvent extraction, ion-exchange, membrane filtration, and adsorption have been used to remove radioactive contaminants from liquid wastes[9–12].

Sorbents are widely employed for industrial wastewater treatment. Application of sorbents allows the recovery of valuable metals at a lower cost than conventional chemical treatment, with a significant saving of space in the treatment plant. Synthetic and natural sorbents and inorganic ion exchangers, such as zeolites[13,14], silicates[15,16], titanosilicates and titanates[17,18], heteropolyacids[19,20] and nanoprous silicates[21–27] compared to the known organic resins, have advantages in terms of higher chemical and thermal stability. In addition, they have specific selectivity for some ions.

As mentioned, Nanoporous silicates like SBA-15[24,25] and MCM-41[26,27] are considered a promising inorganic sorbents for eliminating dangerous substances from liquid waste solutions. This is because of its distinct characteristics such as its extensive surface area of approximately 1500 m^{2}/g, uniform pore sizes ranging from 1.5 to 10 nm, and well-organized nano-channels[28,29]. Borosilicate glasses offer strong chemical resistance and are

[1]Department of Chemistry, University of Maragheh, P.O. Box 5518183111, Maragheh, Iran. [2]Nuclear Science and Technology Research Institute, P. O. Box 11365/8486, Tehran, Iran. ✉email: hsepehrian@aeoi.org.ir

appropriate for immobilizing dangerous radionuclides found in nuclear wastes[30]. Borosilicate glass properties combined with nanoporous MCM-41 can produce an innovative matrix for sorption and secure immobilization of Sr-90.

This paper aims to develop nanoporous aluminoborosilicate as a novel sorbent for Sr ions and as a new matrix for securely immobilizing it. First, the sorption performance of nanoporous AlBS for Sr ions was examined by studying pH impact, sorption kinetics, sorption thermodynamics and sorption isotherms. Afterward, the sorbents loaded with Sr ions were heated at various temperatures to securely immobilize Sr ions. To assess the stability of Sr, a leaching test was conducted on all the samples treated with heat using various eluents.

Materials and methods

Materials

The reagents and chemical substances used in this study, including $SrCl_2.6H_2O$, CsCl, NaCl, $NiCl_2$, $Co(NO_3)_2$, $FeCl_3$, $Al(NO_3)_3.9H_2O$, Na_2SiO_3, H_3BO_3, NaOH, HCl, HNO_3 and H_2SO_4, were of analytical grade and provided by Merck (Darmstadt, Germany), except for cetyltrimethylammonium bromide (CTAB) acquired from Aldrich (Milwaukee, WI, USA).

Preparation of nanoporous aluminoborosilicate

In a typical synthesis of aluminoborosilicate nanoporous[31]. 6 g of CTAB was dissolved in 170 mL doubly deionized water and was continuously mixed at 150 rpm for 15 min, then 30 g of Na_2SiO_3 was added to the solution and was mixed for more 30 min. Then the boric acid solution (5.1 g in 20 mL doubly deionized water) and aluminum nitrate solution (10.7 g in 40 mL doubly deionized water) were added dropwise, respectively. 1 mol./L sodium hydroxide solution was used to adjust the pH of the mixture to 9. After 4 h of continuous stirring, the resulting gel was filtered and thoroughly washed with double deionized water, then the obtained material was dried in an oven at 50 °C for 12 h and calcined in a furnace at 550 °C for 6 h.

Procedure for adsorption tests

Sorption experiments were conducted batch-wise on the nanoporous AlBS sorbent using a 100 mL screw cap bottle. Sr ion solutions (20 mL) with 50 mg/L Sr ion at different pH levels were prepared, and 20 mg of the sorbent was added. The bottles were then placed in a water shaker bath at approximately 150 rpm. Subsequently, the mixture was filtered, and the Sr ion concentration in the aqueous solution were analyzed using atomic absorption spectrometer (AAS) to determine the sorption capacity (q, mg/g) and distribution coefficient (k_d, mL/g) using Eqs. (1) and (2), respectively.

$$q = (C_i - C_f) \times \frac{V}{m} \tag{1}$$

$$K_d = \frac{(C_i - C_f)}{C_f} \times \frac{V}{m} \tag{2}$$

C_i represents the initial concentration of Sr ions, while C_f denotes the final concentration of Sr ions within the solution, measured in mg/L. V stands for the solution's volume in mL, and m indicates the quantity of sorbent used in g.

To study the impact of interfering ions on Sr ion adsorption, 25 ml of a solution containing 0.002 M (175 mg/L) of Sr^{2+} ion, 0.002 M (118 mg/L) of Co^{2+}, 0.004 M (223 mg/L) of Fe^{3+}, 0.01 M (230 mg/L) of Na^+, 0.004 M (235 mg/L) of Ni^{2+}, and 0.002 M (266 mg/L) of Cs^+ was mixed in a 100 ml polyethylene container. After adding 20 mg of the desired adsorbent, the mixture was placed in a shaker set at a temperature of 25 °C and shaken at 150 rpm for 1 h. Then the solution was filtered using filter paper, and the concentration of cesium and Sr ions were measured with an atomic absorption spectrometer and the concentration of cobalt, iron, nickel, and sodium ions were measured with an Inductively Coupled Plasma-Atomic Emission Spectrometers (ICP-AES).

Kinetic, thermodynamic, and isotherm study of Sr ions adsorption

A kinetic analysis was conducted to find kinetic properties for the adsorption of Sr ions onto the nanoporous AlBS sorbent and recognize the stages in the adsorption process. Two models were used to analyze the metal ion sorption kinetics: the pseudo-first-order model (Eq. (3)) and the pseudo-second-order model (Eq. (4))[32]. These models were used to accurately represent the experimental data.

$$q_t = q_e(1 - e^{-k_1 t}) \tag{3}$$

$$q_t = \frac{q_e^2 k_2 t}{1 + q_e k_2 t} \tag{4}$$

q_e represents the equilibrium sorption capacity, q_t represents the sorption capacity at a specific time t (in mg/g), k_1 is the first-order sorption rate constant (in 1/min), and k_2 is the second-order sorption rate constant (in g/(mg.min))[33,34].

The thermodynamic analysis is performed using the van't Hoff equation (Eq. (5))[35].

$$K_d = \exp\left(-\frac{\Delta H^\circ}{RT} + \frac{\Delta S^\circ}{R}\right) \quad (5)$$

The thermodynamic equilibrium constant of adsorption is denoted by K_d, temperature is represented by T in Kelvin, and the universal gas constant is denoted by R (8.314 J/(mol.K)), the enthalpy change is represented by (ΔH°) in J/mol and entropy change is represented by (ΔS°) in J/J/(mol.K).

The Gibbs free energy change (ΔG°) in J/mol, calculated using Eq. (6), is determined[36,37].

$$\Delta G^\circ = \Delta H^\circ - T\Delta S^\circ \quad (6)$$

The Freundlich[38] (Eq. 7), Langmuir[39] (Eq. 8), and Sips[40] (Eq. 9) isotherms are employed to interpret sorption isotherm experimental data. The corresponding model equations are displayed below.

$$q_e = K_F C_e^{\frac{1}{n}} \quad (7)$$

$$q_e = \frac{q_{mL} K_L C_e}{1 + K_L C_e} \quad (8)$$

$$q_e = \frac{q_{mS} K_S C_e^{n_S}}{1 + K_S C_e^{n_S}} \quad (9)$$

q_e represents the equilibrium adsorption amount in mg/g, while C_e stands for the equilibrium concentration of the sorbate in solution in mg/L. Additionally, q_{mL} and q_{mS} denotes the maximum sorption capacity in mg/g for Langmuir and Sips isotherm models, respectively with K_F, K_L, K_S, n and n_S serving as constants specific to the sorbate and sorbent at a particular temperature.

The kinetic, thermodynamic, and isotherm analysis in this study were performed using nonlinear models. The statistical parameters (error functions) employed to evaluate the fitness of these nonlinear models are given in Table 1.

Procedure for immobilization and leach tests

This method involved dispersing 0.4 g of the sorbent in 50 mL of a 0.1 M Strontium solution. The resulting mixture was agitated at approximately 150 rpm at a temperature of 65 °C for 24 h using a water shaker bath. Subsequently, the solution was filtered and sorbent was dried in an oven at 50 °C under ambient pressure. The concentration of Sr ions in the liquid solution was measured using AAS. The amount of Sr ions adsorbed onto the nanoporous AlBS was determined as 10.5 mg of Strontium per 0.4 g of sorbent, through mass balance.

For Strontium immobilization experiments, 0.4 g of Sr-sorbed nanoporous AlBS pellets were created by applying 400 $g.cm^{-2}$ load pressure with a hydraulic press and stainless steel extruder. Subsequently, the pellets underwent thermal treatment at temperatures of 60, 400, 800, and 1100 °C for duration of 2 h. Two methods were employed to characterize the release of Sr from heat-treated samples[5]. (a) 100 mg of the heat-treated Sr-containing nanoporous AlBS was exposed to 50 mL of a 1M sodium chloride solution and agitated for 24 h. Subsequently, the quantity of Sr ions that leached into the aqueous solution was determined using AAS. (b) The heat-treated samples were ground and exposed to distilled water at pH levels of 4 and 7. The pH of the solutions was maintained by adding specific amounts of 0.1 M nitric acid solution. The ratio of solid to liquid weight was 1:50, and the mixture was stirred for 3 h. Following the separation of liquid and solid components, the quantity of Sr ions that had leached out was measured using AAS.

Characterization methods

For characterization of the prepared nanoporous AlBS sample, Fourier transform infrared spectroscopy (FTIR) was employed to record infrared absorption spectra using a Bruker FTIR spectrophotometer model Vector-22 at room temperature with a wavenumber resolution of 1 cm^{-1} using KBr pellets in the frequency range of 4000–400 cm^{-1}. The nitrogen adsorption–desorption studies were conducted using a Quantachrome NOVA 2200e apparatus. The samples were degassed at 383 K in vacuum for 24 h before measurements. The scanning electron microscope Philips XL-30, coupled with energy dispersive spectroscopy (SEM–EDS), was used to analyze the surface morphology and chemical components of the adsorbent. For high resolution scanning electron

Statistical parameters	Equation	
Coefficient of determination (R^2)	$R^2 = \frac{\sum (y_{mean} - y_{cal})^2}{\sum (y_{cal} - y_{mean})^2 + \sum (y_{cal} - y_{exp})^2}$	(10)
Residual sum of squares error (SSE)	$SSE = \sum (y_{exp} - y_{cal})^2$	(11)
Nonlinear chi-square (χ^2)	$\chi^2 = \sum \frac{(y_{exp} - y_{cal})^2}{y_{cal}^2}$	(12)
Hybrid fractional error function (HYBRID)	$HYBRID = \frac{100}{N_{exp} - N_{para}} \sum \frac{y_{exp} - y_{cal}}{y_{exp}}$	(13)
Root Mean Square Error(RMSE)	$RMSE = \sqrt{\frac{1}{N_{exp}} \sum (y_{exp} - y_{cal})^2}$	(14)

Table 1. Statistical parameters for non-linear models fitting.

microscopy, the samples have been coated with a gold layer (3 nm) by conventional sputtering to avoid charging. The JEM 1200 EX apparatus with a 100 kV acceleration voltage captured the TEM image of the nanoporous AlBS sample. XRD analysis characterized the crystal structure of the sample, using a STOE (STDI MP) system with a Cu-kα_1 source ($\lambda = 0.15406$ nm, 40 kV, 30 mA) for X-ray diffraction. The diffraction patterns were recorded in the 2θ range of 1–10° with a step size of 0.02° and a step time of 5 s. X'Pert software was used for the single line fitting of the XRD peaks. A Varian Liberty 150 AX Turbo model inductively coupled plasma-atomic emission spectroscopy (ICP-OES) and Varian SPECTRA AA-200 atomic absorption spectroscopy (AAS) was used for the determination of metal ions.

Results and discussion

Characterization of the nanoporous AlBS

The presence of a strong peak at 2θ smaller than 3° in the low-angle XRD pattern of nanoporous AlBS confirms the formation of a structure similar to MCM-41[28,29]. The unit cell parameter a_0 and spacing d of nanoporous AlBS are given in Table 2. Also, the typical adsorption profile of type IV in the nitrogen adsorption–desorption isotherm of nanoporous AlBS confirms the formation of a structure similar to MCM-41[28,29]. The porosity characteristics of the prepared nanoporous AlBS sample are given in Table 2. Results show that the nanoporous AlBS sample provides 485 m^2/g specific surface areas.

More details including the low angle XRD pattern, nitrogen sorption and desorption isotherms and pore size distribution, FTIR spectra, SEM image and EDX spectrum pattern, and TEM images of the nanoporous AlBS matrix presented in our previously published paper[31], are given in the Supplementary Information section (see Supplementary Figs. S1, S2, S3, S4, and S5).

Results of adsorption tests

Effect of the contact time (Kinetic analysis)

The sorption kinetics of a sorbent is crucial in determining its effectiveness. Therefore, the kinetic analysis is necessary to gather crucial data, assess the sorbent's viability for use in treatment systems, and determine the best operating conditions for the batch process. The study examined how the equilibration time affects Sr ions sorption onto nanoporous AlBS matrix. Findings from Fig. 1 reveal that Sr ions sorption rises as contact time increases, reaching equilibrium after 60 min.

Each adsorption process can adhere to one of the different patterns including chemical reactions, diffusion control, mass transfer, or a combination of these factors. Examining the experimental data over different time intervals allows for the calculation of kinetic parameters and provides valuable information for the design and modeling of the adsorption processes. Table 3 displays kinetic adsorption parameters obtained using pseudo-first-order and pseudo-second-order models. According to the obtained data, inadequate statistical parameters

Sample	XRD d_{100} (A°)	unit cell parameter a_0 (A°)	Surface area (m^2/g)	Pore volume (mL/g)	Pore size (nm)
Nanoporous AlBS	34.67	40.03	485	0.28	2.20, 3.60

Table 2. The physical and porosity characteristics of the synthesized nanoporous AlBS[31].

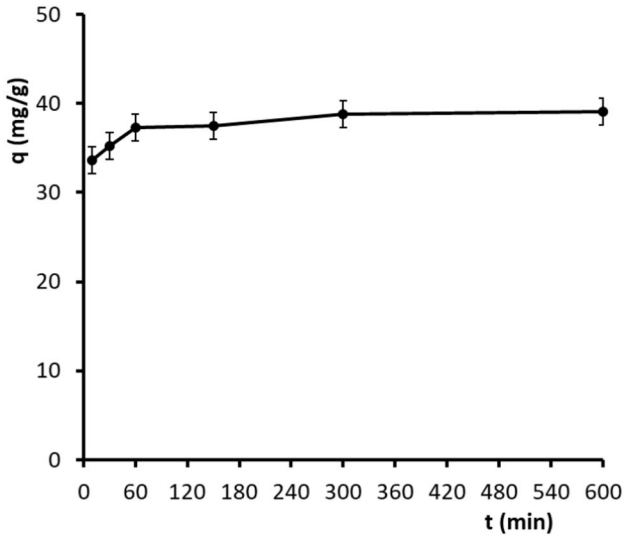

Fig. 1. Effect of contact time on the sorption of Sr ions by nanoporous AlBS sorbent (Sr ions concentration = 50 mg/L, pH = 5, S/V = 0.8, T = 25 °C).

Kinetic model	Pseudo first order (PFO)	Pseudo second order (PSO)
Parameters	q_e (mg/g) = 37.60	q_e (mg/g) = 38.43
	k_1 (1/min) = 0.22	k_2 (g/(mg min)) = 0.016
Statistical parameters		
R^2	0.92	0.99
SSE	9.33	3.08
χ^2	0.25	0.08
HYBRID	− 0.009	− 0.012
RMSE	1.15	0.66

Table 3. Kinetic adsorption parameters obtained using pseudo-first-order and pseudo-second-order models (Sr ions concentration = 50 mg/L, pH = 5, S/V = 0.8, T = 25 °C).

corresponding to the pseudo-first-order kinetic model indicate that the Sr ion sorption process does not adhere to the PFO model. A higher R^2 value and the lower SSE, χ2, HYBRID, and RMSE values for pseudo-second-order kinetic model confirm that the sorption data aligns with the PSO model. Additionally, the qe value calculated for PSO is significantly close to those determined through experimental measurements, reinforcing the earlier conclusion. As per this model, both Sr ions and nanoporous AlBS sorbent concentrations affect the rate-controlling step of the sorption process[41].

The effect of solution pH

The adsorption of Sr ions onto nanoporous AlBS sorbent may be significantly impacted by the pH of the solution, which influences both the binding sites (such as the level of protonation) and the behavior of Sr ions in the water (such as precipitation). To find the best pH for Sr ions adsorption, solutions with different pH levels ranging from 2.5 to 10.0 were acquired. From the Sr ions speciation diagram, Sr^{2+} is the predominant species in the investigated pH range[5]. Figure 2 illustrates the impact of solution pH on Sr ions adsorption by the nanoporous AlBS sorbent. The adsorption of H^+ ions onto nanoporous AlBS protonated the sorbent's surface and decreased the electrostatic interaction, resulting in reduced Sr ions sorption capacities at lower solution pH levels. The Sr ions adsorption on the nanoporous AlBS sorbent significantly increases from 6.25 mg/g to 48.62 mg/g between pH 2.5 and 5.5. Substituting trivalent aluminum and boron atoms for tetravalent silicon within the MCM-41 structure produced a nanoporous AlBS sorbent with negative charges. As a result, the nanoporous AlBS sorbent can serve as an inorganic cation exchanger, efficiently capturing Sr ions from liquid waste solutions.

In acidic solutions (pH < 2), there is often an abundance of H^+ ions, which can compete with Sr^{2+} ions for adsorption sites on the aluminoborosilicate surface. The surface of aluminoborosilicate tends to become more protonated, meaning it has more positive charge due to the adsorption of H^+ ions. This positive surface charge

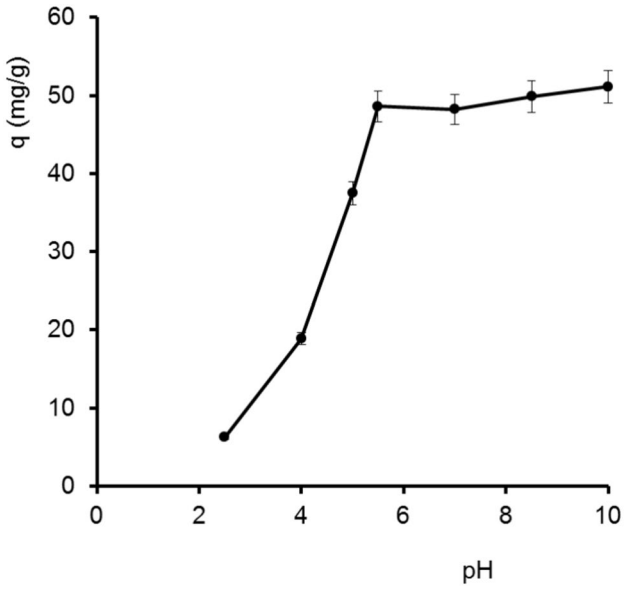

Fig. 2. Effect of solution pH on the sorption of Sr ions by nanoporous AlBS sorbent (Time = 60 min, Sr ions concentration = 50 mg/L, S/V = 0.8, T = 25 °C).

can create electrostatic repulsion between the surface and the Sr^{2+} ions, which are also positively charged. As a result, the adsorption of strontium is typically reduced under acidic conditions.

At higher pH levels, the surface of aluminoborosilicate becomes deprotonated, resulting in a more negatively charged surface. The negative charge on the surface enhances the attraction of Sr^{2+} ions, leading to increased adsorption. Therefore, strontium adsorption is generally more effective at higher pH levels.

In most pH ranges encountered during adsorption processes (typically pH 4–9), strontium exists predominantly as free Sr^{2+} ions. However, at very high pH (above 10–11), strontium can start to form hydroxide complexes (e.g., $Sr(OH)^{+}$), although this is less common.

Optimal conditions for Sr^{2+} adsorption, where the aluminoborosilicate surface is more negatively charged (pH 5.5–10), enhancing electrostatic attraction and ion exchange. In this study, we selected the lowest optimal pH level of 5.5.

Effect of temperature (Thermodynamic analysis)

The impact of temperatures at 25, 35, 45, 55, and 65 °C on the sorption behavior of Sr ions onto nanoporous AlBS sorbent was assessed (Fig. 3). Findings indicated a slight increase in Sr ions' sorption from 45.8 mg/g to 53.2 mg/g as the temperature rose from 25 to 65 °C. This pertains to improving the sorbent's effective sorption sites and facilitating the diffusion of Sr ions at elevated temperatures.

The thermodynamic details of the Sr adsorption process and the corresponding statistical parameters can be found in Table 4.

Based on the results, the sorption process of Sr was found to be spontaneous due to the negative ΔG° values. Additionally, the positive ΔH° value indicated that the process is endothermic, while the ΔS° value suggests feasibility and randomness at the solution and sorbent interface. In our study, the calculated value for ΔG° indicates that the sorption of Sr ions onto nanoporous AlBS sorbent involves a physisorption process[42].

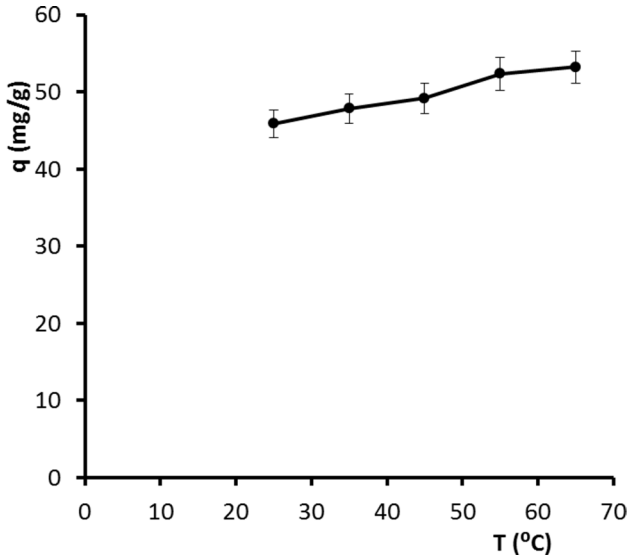

Fig. 3. Effect of temperature on the sorption of Sr ions by nanoporous AlBS sorbent (Time = 60 min, Sr ions concentration = 50 mg/L, pH = 5.5, S/V = 0.8).

		ΔH° (kJ/mol)	ΔS° (kJ/(mol.K))
Parameters		**18.54**	**0.071**
Statistical parameters		ΔG° (kJ/mol)	
R^2	0.97	298 K	−2.63
SSE	0.36	308 K	−3.35
χ^2	0.07	318 K	−4.06
HYBRID	−0.42	328 K	−4.77
RMSE	0.27	338 K	−5.48

Table 4. Thermodynamic parameters of Sr ions adsorption onto nanoporous AlBS sorbent at different temperatures (Time = 60 min, Sr ions concentration = 50 mg/L, pH = 5.5, S/V = 0.8).

Effect of initial metal ion concentration (isotherm analysis)

Designing a sorption system relies on having equilibrium data, also called sorption isotherms. The effect of Sr ions initial concentration in the range of 5 to 300 mg/L on the adsorption capacity of AlBS sorbent was investigated. Figure 4 shows the experimental data alongside the Langmuir, Freundlich, and Sips isotherm models. The isotherm parameters for Sr ions adsorption onto nanoporous AlBS sorbent obtained from the nonlinear regression and calculated statistical parameters are presented in Table 5. According to these results, the Sips isotherm model showed better agreement with the experimental data compared to the Langmuir and Freundlich models. The Sips isotherm model is the most applicable 3-parameter model incorporating Langmuir and Freundlich expressions for representing the equilibrium adsorption data[40]. Sips model can describe both homogeneous and heterogeneous systems and is employed to avoid limiting the rising adsorbate concentration associated with the Freundlich isotherm model. The sips model suggests that the sorption process is related the monolayer adsorption of one adsorbate molecule onto $1/n_s$ adsorption sites. The maximum adsorption capacity (q_{max}) of nanoporous AlBS sorbent was determined as 163.08 mg/g based on the evaluated parameters for the Sips model (Table 5).

Effect of interfering ions on Sr ions adsorption

The impact of sodium, cesium, nickel, cobalt, and iron cations on q and k_d was examined to evaluate the selectivity of nanoporous AlBS sorbent under optimal conditions for Sr ions adsorption. The relevant data can be found in Table 6. Cesium and Sodium ions have a greater impact on the adsorption of Sr ions on nanoporous AlBS compared to other ions. The study revealed that the adsorbent's overall capacity is 678.50 mg/g, with Cs ions and Sr ions having individual adsorption capacities of 238.13 mg/g and 237.50 mg/g, respectively, when accompanied by cations.

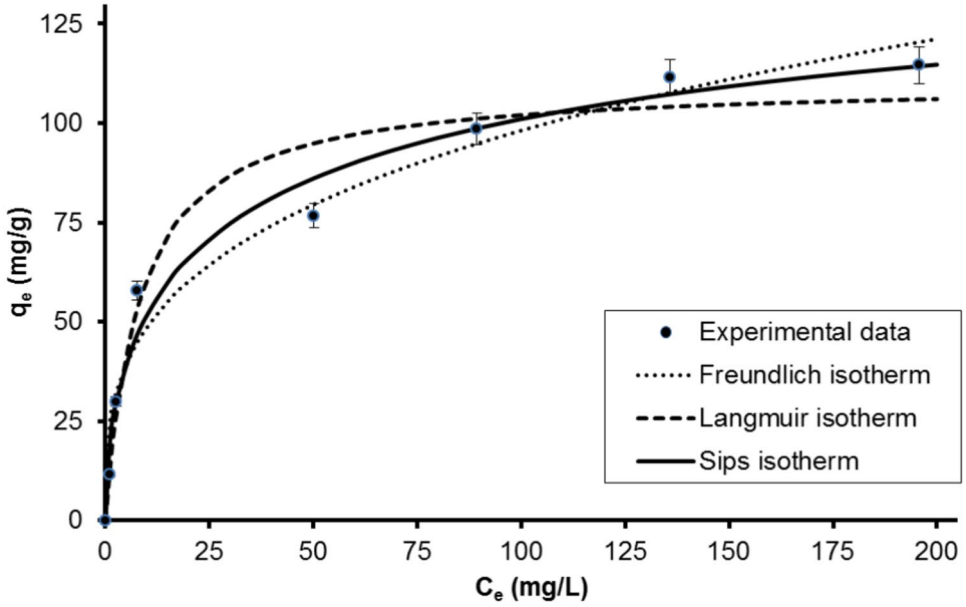

Fig. 4. Isotherm analysis of Sr ions adsorption onto nanoporous AlBS sorbent plot (Time = 60 min, pH = 5.5, S/V = 0.8, T = 25 °C).

Isotherm model	Freundlich	Langmuir	Sips
	K_f ($L^1/(mg^{1-1/n}.g)$) = 24.21	q_m (mg/g) = 110.41	q_{ms} (mg/g) = 163.08
			K_s $(L/mg)^{nS}$ = 0.13
Parameters	n = 3.29	K_L (L/mg) = 0.12	n_S = 0.54
Statistical parameters			
R^2	0.97	0.96	0.98
SSE	413.58	499.73	294.53
χ^2	11.49	5.72	7.18
HYBRID	5.42	− 1.15	4.89
RMSE	7.19	7.90	6.07

Table 5. Isotherm parameters for Sr ions adsorption onto nanoporous AlBS sorbent.

Cations	Sr^{2+}	Fe^{3+}	Co^{2+}	Ni^{2+}	Cs^{+}	Na^{+}
K_d (mL/g)	896.23	77.78	155.71	178.80	881.94	722.69
q (mg/g)	237.50	35.00	20.34	37.72	238.13	109.81

Table 6. Comparison of adsorption of Sr ion and interfering ions onto nanoporous AlBS.

Iron (III), cobalt (II) and nickel (II) ions have a high charge density because of their large charge and relatively small ionic radius (~0.55–0.75 Å in a six-fold coordination). This high charge density can lead to strong interactions with oxygen atoms, but also make Fe^{3+}, Co^{2+} and Ni^{2+} less compatible with the aluminoborosilicate network where lower charge cations (like Na^{+}, Cs + and Sr^{2+}) are more easily accommodated. The aluminoborosilicate network is composed of SiO_4, AlO_4, and BO_4 tetrahedral, which form a rigid and stable framework. Fe^{3+}, Co^{2+} and Ni^{2+} due to its high charge and specific coordination preferences (often octahedral rather than tetrahedral), may not easily fit into the network's available sites, leading to lower adsorption.

Comparison with other similar sorbents

Table 7 summarizes the comparison of Sr ions adsorption from various aqueous solutions using different sorbents as documented in studies[23–27], alongside the newly introduced nanoporous AlBS sorbent. Based on the reported q_{max} values, the nanoporous AlBS prepared in this study had a higher sorption capacity compared to previous findings. Additionally, the S/V = 0.8 g/L used in this research had the lowest value among existing studies.

Leaching test

Figure 5 shows a comparison of the quantities of Sr ions released from the heat-treated nanoporous AlBS matrix by various eluents based on the treatment temperature. In a solution containing 1 M NaCl as an eluent, the samples treated at 60 and 400 °C showed poor stabilization ability, and 100% and 63.81% of the initially adsorbed Sr^{2+}

Adsorbent	q_{max} (mg/g)	S/V (g/L)	References
Mesoporous silica (MS)	89.19	–	[23]
SBA-15	17.67	0.06/0.06 = 1	[24]
SBA-15[a]	73.90	0.1/0.01 = 10	[25]
MCM-41	9.97	0.05/0.01 = 5	[26]
MCM-41[b]	97.09	0.02/0.02 = 1	[27]
nanoporous AlBS sorbent	163.08	0.02/0.025 = 0.8	Present work

Table 7. Comparison of the present work results with the previous studies on the adsorption of Sr ions from aqueous solutions. [a]Mesoporous SBA-15 modified with Tin (IV) molybdophosphate. [b]Meoporous MCM-41 modified with Lead hexacyanoferrate.

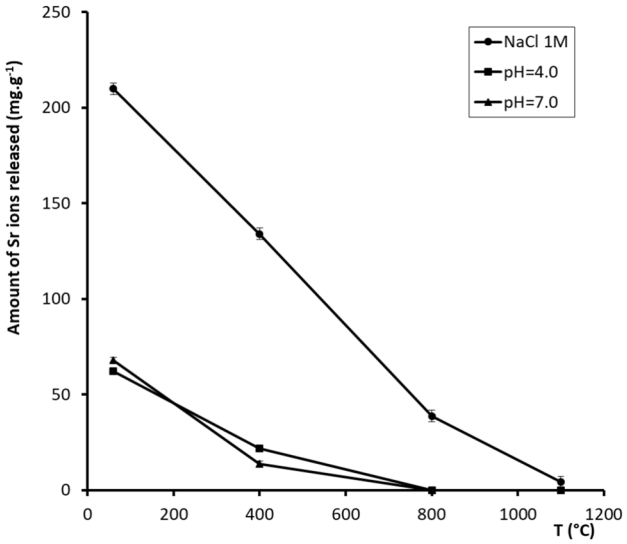

Fig. 5. Amount of Sr ions released by heat-treated samples contacted with different eleunts, as a function of the treatment temperature.

were released, respectively. An increase in treatment temperature improved the ability to stabilize. The thermal treatment at about 1100 °C provides effective stabilization, as just 3.43% of the originally absorbed Sr ions was released. When the Sr-loaded nanoporous AlBS is heated to approximately 1100 °C, the silicate structure breaks down and forms an amorphous, likely glassy phase. This phase effectively encloses the Sr ions, as shown by leaching tests. In an aqueous solution with pH levels of 4 and 7 as the eluent for the availability test, Sr ions was not detected even at temperatures as low as 800 °C. Figure 6a,b represent the SEM image and the EDX spectrum of the nanoporous AlBS matrix after Sr ions stabilization at about 1100 °C. The SEM image clearly displays the glass phase that has developed on the surface of the nanoporous AlBS matrix. Additionally, the EDX spectrum validates the existence of Strontium within the glass phase, suggesting that Sr ions has not evaporated due to heat.

Conclusions

This research aimed to enhance the surface area of the aluminosilicate adsorbent by introducing porosity into its structure, thereby improving strontium ions adsorption by optimizing the adsorption conditions. Furthermore, the addition of boron to the aluminosilicate framework was investigated to enhance strontium stabilization during heat treatment, ultimately leading to the formation of a borosilicate glass structure. The peapaerd nanoporous aluminoborosilicate demonstrated a maximum sorption capacity of 163.08 mg/g under optimal conditions (pH = 5.5, contact time = 60 min, temperature = 25 °C), surpassing the sorption capacities of previously reported similar adsorbents in the literature. The findings of thermal treatment at different temperatures revealed that as the temperature increased from 60 to 1100 °C, the amount of strontium ions released, decreased from 100% to 3.43%. Our research shows that the developed matrix can efficiently manage liquid radioactive wastes containing strontium.

Data availability

The datasets used and/or analyzed during the current study are available from the corresponding author on reasonable request.

Received: 18 June 2024; Accepted: 4 September 2024
Published online: 16 September 2024

References

1. Liguori, B., Caputo, D., Iucolano, F., Aprea, P. & de Gennaro, B. Entrapping of Cs and Sr in heat-treated zeolite matrices. *J. Nucl. Mater.* **435**, 196–201 (2013).
2. Shimura, H. *et al.* Absorption of radionuclides from the Fukushima nuclear accident by a novel algal strain. *PLoS ONE* **7**, e44200 (2012).
3. Steinhauser, G., Schauer, V. & Shozugawa, K. Concentration of strontium-90 at selected hot spots in Japan. *PLoS ONE* **8**, e57760 (2013).
4. Fukuda, S.-Y. *et al.* Global searches for microalgae and aquatic plants that can eliminate radioactive cesium, iodine and strontium from the radio-polluted aquatic environment: A bioremediation strategy. *J. Plant. Res.* **127**, 79–89 (2014).
5. Höllriegl, V. & München, H. Strontium in the environment and possible human health effects. *Encycl. Environ. Health* **5**, 268–275 (2011).
6. Amata, R., Diamond, G. L., Dorsey, A. & Fransen, M. E. Toxicological profile for strontium. (2004).
7. Suarez, D. L. Beryllium, magnesium, calcium, strontium, and barium. *Methods Soil Anal. Part 3 Chem. Methods* **5**, 575–601 (1996).
8. Skougstad, M. W. & Horr, C. A. *Occurrence and distribution of strontium in natural water*. (US Government Printing Office, 1963).
9. Pacary, V., Barré, Y. & Plasari, E. Method for the prediction of nuclear waste solution decontamination by coprecipitation of strontium ions with barium sulphate using the experimental data obtained in non-radioactive environment. *Chem. Eng. Res. Des.* **88**, 1142–1147 (2010).

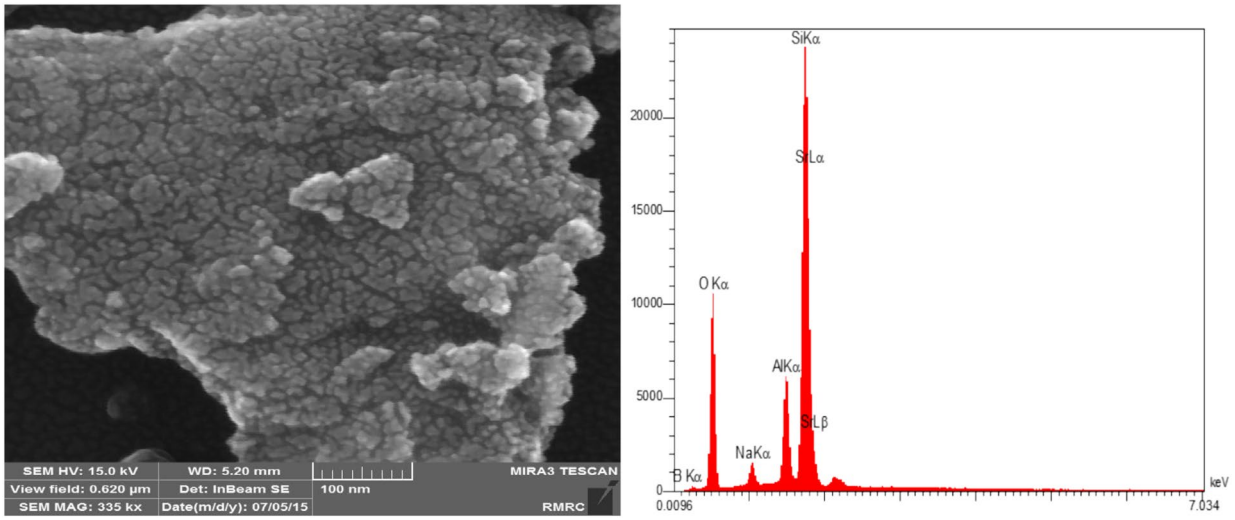

Fig. 6. SEM image and EDX area analysis of the heat-treated Sr-containing nanoporous AlBS matrix at about 1100 °C.

10. Zhang, A., Chen, C., Kuraoka, E. & Kumagai, M. Impregnation synthesis of a novel macroporous silica-based crown ether polymeric material modified by 1-dodecanol and its adsorption for strontium and some coexistent metals. *Sep. Purif. Technol.* **62**, 407–414 (2008).
11. Zhang, A. Y., Akashi, T., Zhang, B. P. & Goto, T. Electrical conductivity of partially ion exchanged Sr and Ba β-alumina single crystals determined by ac impedance spectroscopy. *Mater. Lett.* **60**, 2834–2836 (2006).
12. Rao, S., Paul, B., Lal, K., Narasimhan, S. & Ahmed, J. Effective removal of cesium and strontium from radioactive wastes using chemical treatment followed by ultra filtration. *J. Radioanal. Nuclear Chem.* **246**, 413–418 (2000).
13. Sabriye, Y. & Sema, E. Adsorption characterization of strontium on PAN/zeolite composite adsorbent. *World J. Nuclear Sci. Technol.* **2011**, 6–12 (2011).
14. Seliman, A., Lasheen, Y., Youssief, M., Abo-Aly, M. & Shehata, F. Removal of some radionuclides from contaminated solution using natural clay: Bentonite. *J. Radioanal. Nuclear Chem.* **300**, 969–979 (2014).
15. Gordienko, P. *et al.* Sorption of strontium ions on barium silicates from solutions of complex salt composition. *Russ. J. Inorg. Chem.* **64**, 1579–1586 (2019).
16. Yarusova, S. *et al.* Study of strontium sorption by amorphous calcium silicate. *Russ. J. Inorg. Chem.* **67**, 1386–1392 (2022).
17. Noh, Y. D., Komarneni, S. & Mackenzie, K. J. Titanosilicates: Giant exchange capacity and selectivity for Sr and Ba. *Sep. Purif. Technol.* **95**, 222–226 (2012).
18. Duff, M. *et al.* Mechanisms of strontium and uranium removal from high-level radioactive waste simulant solutions by the sorbent monosodium titanate. *Environ. Sci. Technol.* **38**, 5201–5207 (2004).
19. Marageh, M., Husain, S. & Khanchi, A. Selective sorption of radioactive cesium and strontium on stannic molybdophosphate ion exchanger. *Appl. Radiat. Isot.* **50**, 459–465 (1999).
20. Neudachina, L. K. & Barkovskii, V. F. Sorption mechanism of metal ions on the salts of heteropoly acids. *Russ. Chem. Rev.* **50**, 793 (1981).
21. Faghihian, H., Nasri Nasrabadi, S. & Khonsari, S. Removal of Sr (II) from aqueous solutions by aminosilane functionalized MCM-48. *Sep. Sci. Technol.* **49**, 2031–2038 (2014).
22. Leng, Y. *et al.* Synthesis of new periodic mesoporous organosilica (PMO) incorporated with macrocyclic host for strontium binding. *Mater. Let.* **110**, 212–214 (2013).
23. Attia, M. A., Hamoud, M. A., Ghamry, M. A. & Mahmoud, M. R. Fast and effective sorption of radioactive Sr (II) onto mesoporous silicate. *Radiochimica Acta* **111**, 533–543 (2023).
24. Zhang, N. *et al.* Adsorption of strontium from aqueous solution by silica mesoporous SBA-15. *J. Radioanal. Nuclear Chem.* **303**, 1671–1677 (2015).
25. Aghayan, H., Mahjoub, A. & Khanchi, A. Immobilization of Tin (IV) molybdophosphate onto mesoporous silica SBA-15 and its application on strontium removal from aqueous solution. *Appl. Surf. Sci.* **261**, 14–20 (2012).
26. Sarı Yılmaz, M., Dere Özdemir, Ö. & Pişkin, S. Synthesis and characterization of MCM-41 with different methods and adsorption of Sr 2+ on MCM-41. *Res. Chem. Intermed.* **41**, 199–211 (2015).
27. Vashnia, S., Tavakoli, H., Cheraghali, R. & Sepehrian, H. Supporting of lead hexacyanoferrate on mesoporous MCM-41 and its use as effective adsorbent for strontium: Equilibrium, kinetic, and thermodynamic studies. *Sep. Sci. Technol.* **49**, 241–248 (2014).
28. Kresge, A. C., Leonowicz, M. E., Roth, W. J., Vartuli, J. & Beck, J. Ordered mesoporous molecular sieves synthesized by a liquid-crystal template mechanism. *Nature* **359**, 710–712 (1992).
29. Beck, J. S. *et al.* A new family of mesoporous molecular sieves prepared with liquid crystal templates. *J. Am. Chem. Soc.* **114**, 10834–10843 (1992).
30. Plodinec, M. Borosilicate glasses for nuclear waste imobilisation. *Glass Technol.* **41**, 186–192 (2000).
31. Abbasi, A. *et al.* Development of nanoporous alumino-borosilicate as a novel matrix for the sorption and stable immobilization of cesium ions. *J. Inorg. Organomet. Polym. Mater.* **30**, 369–378 (2020).
32. Revellame, E. D., Fortela, D. L., Sharp, W., Hernandez, R. & Zappi, M. E. Adsorption kinetic modeling using pseudo-first order and pseudo-second order rate laws: A review. *Clean. Eng. Technol.* **1**, 100032 (2020).
33. Tavakoli, H., Sepehrian, H. & Cheraghali, R. Encapsulation of nanoporous MCM-41 in biopolymeric matrix of calcium alginate and its use as effective adsorbent for lead ions: Equilibrium, kinetic and thermodynamic studies. *J. Taiwan Inst. Chem. Eng.* **44**, 343–348 (2013).
34. Cheraghali, R., Tavakoli, H. & Sepehrian, H. Preparation, characterization and lead sorption performance of alginate-SBA-15 composite as a novel adsorbent. *Scientia Iranica* **20**, 1028–1034 (2013).
35. Lima, E. C., Gomes, A. A. & Tran, H. N. Comparison of the nonlinear and linear forms of the van't Hoff equation for calculation of adsorption thermodynamic parameters (Δ S° andΔ H°). *J. Mol. Liq.* **311**, 113315 (2020).
36. Hamed, M. M., Holiel, M. & Ahmed, I. Sorption behavior of cesium, cobalt and europium radionuclides onto hydroxyl magnesium silicate. *Radiochimica Acta* **104**, 873–890 (2016).
37. Zheng, S., Gao, L., Zhang, Q.-H. & Guo, J.-K. Synthesis, characterization and photocatalytic properties of titania-modified mesoporous silicate MCM-41. *J. Mater. Chem.* **10**, 723–727 (2000).
38. Freundlich, H. Über die adsorption in lösungen. *Zeitschrift für physikalische Chemie* **57**, 385–470 (1907).
39. Langmuir, I. The constitution and fundamental properties of solids and liquids. Part I. Solids. *J. Am. Chem. Soc.* **38**, 2221–2295 (1916).
40. Sips, R. On the structure of a catalyst surface. *J. Chem. Phys.* **16**, 490–495 (1948).
41. Liu, C.-C., Kuang-Wang, M. & Li, Y.-S. Removal of nickel from aqueous solution using wine processing waste sludge. *Ind. Eng. Chem. Res.* **44**, 1438–1445 (2005).
42. Rao, M. M., Rao, G. C., Seshaiah, K., Choudary, N. & Wang, M. Activated carbon from Ceiba pentandra hulls, an agricultural waste, as an adsorbent in the removal of lead and zinc from aqueous solutions. *Waste Manag.* **28**, 849–858 (2008).

Author contributions

Ali Abbasi: data collection. Armen Avanes: study conception and design. Reza Davarkhah: data collection. Ali Yadollahi: analysis and interpretation of results, draft manuscript preparation. Hamid Sepehrian: study conception and design, analysis and interpretation of results, draft manuscript preparation.

Competing interests

The authors declare no competing interests.

Additional information

Supplementary Information The online version contains supplementary material available at https://doi.org/10.1038/s41598-024-72126-3.

Correspondence and requests for materials should be addressed to H.S.